ISBN: 978-3-95450-261-5 ISSN: 2673-7000 doi: 10.18429/JACoW-NAPAC2025-MOP086

SEM GRID TESTING AT NLCTA IN BEAMNETUS PROGRAM*

A. Baxter[1], A. Dhar[2], A. Gabriel[2], D. McCormick[2], E. Kendrick[1], E. Snively[2], G.A. Klinger[1], J. Cruz[2], N. Horiguchi[1], N. Samuel[1,2,†], S. Allen[1], W.H. Tan[2], D. Nembhard[1]
[1]Harvey Mudd College, Claremont, CA, USA
[2]SLAC National Accelerator Laboratory, Menlo Park, CA, USA

Abstract

We report on the performance of a secondary electron monitor (SEM) grid used to measure the transverse profile of an MeV range electron beam tested at SLAC National Accelerator Laboratory's Next Linear Collider Test Accelerator (NLCTA) facility. When inserted into the path of the electron beam, secondary electron emission results in a measurable current on the wires that make up the grid. We present measurements using this technique to reconstruct the beam profile. The SEM grid was designed and manufactured by a team of undergraduate students at Harvey Mudd College (HMC) and was tested at SLAC's NLCTA facility in collaboration with NCLTA staff as part of the BeamNetUS program. Developed for real-time diagnostics of MeV-range electron beams, this SEM grid has potential applications in both industrial and medical contexts.

INTRODUCTION

Secondary electron emission monitors (SEM) grids are well-established devices for determining the transverse profile of particle beams. Examples include designs for use with proton beams at Fermilab [1], and for electron beams at DESY [2].

The SEM grid tested in this experiment was designed as part of an undergraduate engineering capstone project at Harvey Mudd College. The goal was to design a device to capture and transmit real-time data on the transverse profile of an electron beam for NorthStar Medical Radioisotopes, the capstone project sponsor. NorthStar is a radiopharmaceutical company who produces radioisotopes Actinium-225 and Copper-67 for cancer treatment [3]. These radioisotopes are produced through a process including irradiation of target materials with an IBA Rhodotron electron beam [4, 5].

One of the prototypes developed as part of this project was tested at SLAC National Laboratory's Next Linear Collider Test Accelerator (NLCTA) facility. The X-band Test Accelerator (XTA) at NLCTA provided a comparable electron beam energy to NorthStar's IBA Rhodotron but at a significantly lower power (< 1 W). At this low power, the functionality of the prototype could be tested without the challenges associated with excessive heating. The following sections describe general principles of SEM grids, the design of our specific prototype, the experimental setup and procedure, and the analysis and conclusions from the data.

*This work was supported by the U.S. Department of Energy, Accelerator R&D and Production Program, under Contract No. DE-AC02-76SF00515 as part of BeamNetUS.
†nsamuel@g.hmc.edu

SEM GRID BACKGROUND

SEM grids work by the phenomenon of secondary electron emission (SEE), which occurs when an incident particle beam imparts sufficient energy to a target material such that electrons escape the material entirely, leaving a charge behind [6–8]. In the case of an SEM grid setup, the target material of interest is one or two grids of wires which the beam is incident on. When the beam hits these wires, the energy transfer frees some electrons from the wires. This results in a measurable current in each of the wires, varying across the cross section of the beam and grid [9]. Biasing, the introduction of a large voltage to the setup, is often used to control the potential re-absorption of emitted electrons back into the wires [2, 6].

Based on the literature on SEM grids, we developed a prototype consisting of one vertical and one horizontal wire frame, and three biasing plates. The wire frames each had six tungsten wires, spaced approximately 0.2" apart. The wire diameter was less than a millimeter, and was chosen through thermal analysis.

EXPERIMENTAL PROCEDURE

The SEM grid set-up in the NLCTA beamline was configured for quick accessibility. The SEM grid and biasing plates were enclosed in a plastic box to make the device touch safe, as shown in Fig. 1 at left. The SEM grid was mounted on a two-axis translation stage in air at the end of the beamline. A DRZ screen [10], serving as an alternative beam profile monitor, was placed on the stage on top of the SEM grid prototype in the approximate plane of the wires, as seen in Fig. 1 at right. A smaller piece of DRZ was placed near the entrance to the SEM grid assembly to assist with initial alignment of the beam into the enclosure.

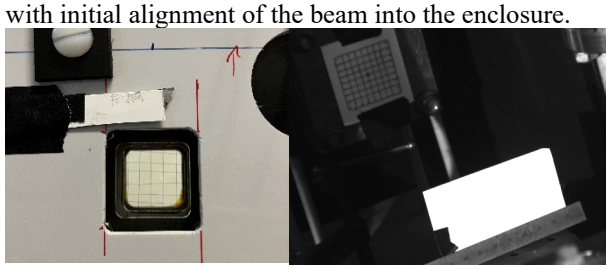

Figure 1: SEM grid with both wire grids visible through aperture in plastic enclosure, and alignment DRZ film above aperture (left) the DRZ film (bright white rectangle) illuminated on top of the plastic enclosure, in the same camera frame used to image the beam profile (right).

The electrical current signal from each individual wire of the SEM grid was passed through long BNC cabling out of the beam area to the control room and then to a SR750

ISBN: 978-3-95450-261-5 ISSN: 2673-7000 doi: 10.18429/JACoW-NAPAC2025-MOP086

preamplifier. This amplifier filtered the signal and converted it from a low current to an oscilloscope-readable voltage. This conversion was either on a 10 pA/V setting or a 200 pa/V setting, depending on the signal. The output voltage was then measured using an oscilloscope. The biasing plates were positively biased to prevent emitted electrons from returning to the wires.

The electron beam exited the vacuum of the XTA beampipe through a 50 µm beryllium window before propagating for about 60 cm to reach the SEM grid. Real time images of the fluorescence from the DRZ in the beam path could then be compared with the SEM grid measurements, as each diagnostic was moved into the path of the beam using the two-axis stage. An image of the DRZ screen is shown in the right panel of Fig. 1 with a ruler for establishing pixel size.

The electron beam from XTA was dominated by dark current, resulting in a large energy spread peaking at 50 MeV. The total charge was approximately 3 pC with an oblong profile as shown in Fig. 2. The large beam size helped to ensure there were distinguishing features in the beam profile that could potentially be resolved by the wires of the SEM grid.

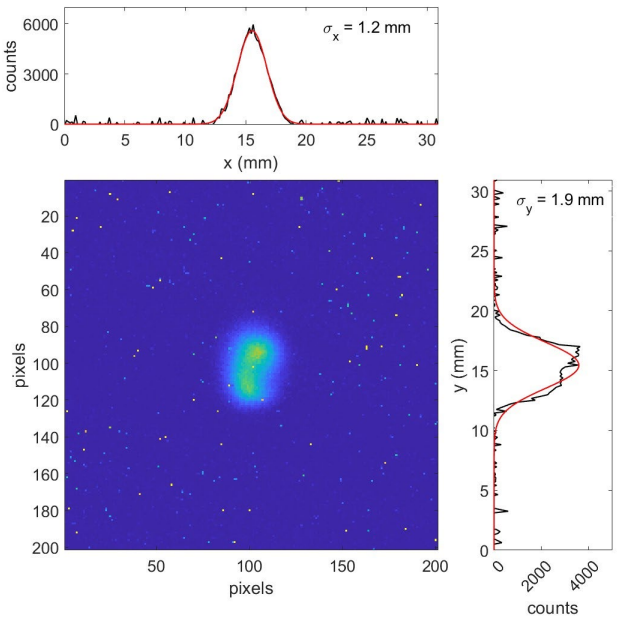

Figure 2: Electron beam profile on the DRZ screen in air. Above and at right are the projected pixel sums along each axis with a Gaussian fit.

EXPERIMENTAL RESULTS AND DATA ANALYSIS

SEM grid measurements for the 2D beam profile were collected using the hardware assembly shown in Fig. 1, with horizontal and vertical wires supported on two separate frames and three biasing plates. Data were collected from three wires on each frame, one at a time. Collection of more data points was limited by challenges with simultaneous signal readout, requiring multiple accelerator housing accesses to change connections to measure each wire. The large spacing between wires relative to overall beam size also limited the resolution of the profile diagnostic.

To reconstruct a 2D profile from the SEM grid, we first fitted a Gaussian distribution to the beam measurements in both axes and constrained the background to zero. The fitting routine could not calculate covariance because of the low number of data points. The resulting profiles with fitted Gaussians for each wire plane are shown on the side panel graphs in Fig. 3. The 2D profile in the center of Fig. 3 is the normalized outer product of these fitted Gaussians.

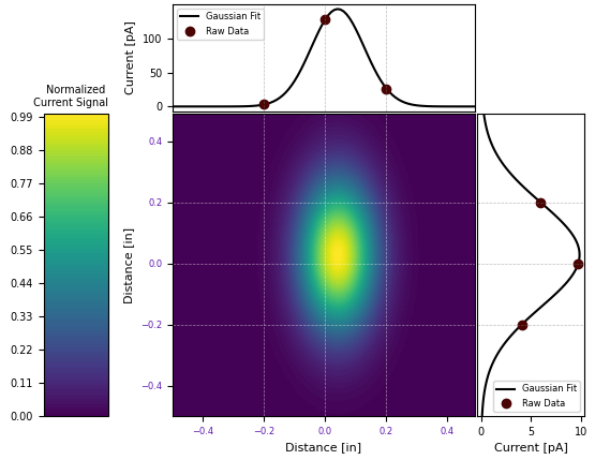

Figure 3: Reconstructed profile from the SEM grid data, assuming a Gaussian distribution of the beam in both the horizontal and vertical wire grids. The 2D representation is the normalized outer product of the fitted Gaussians on the side panels.

The two profiles observed in the DRZ image, Fig. 2, and the reconstructed SEM grid profile, Fig. 3, are similarly shaped, showing an oblong beam distribution. The resolution of the SEM grid wires is not sufficient to resolve features within the beam profile. The SEM reconstructed grid profile indicates a FWHM of about 10 mm by 5 mm, whereas the DRZ image shows a FWHM of 5.3 mm by 2.8 mm. Without additional data points from the SEM grid, it is difficult to determine the cause of the discrepancy between the size in these two measurements. The SEM grid data analysis for reconstructing the profile does not account for the misalignment of wires within the SEM grid, visible in Fig. 1, which contributes to uncertainty in the appropriate spacing of the data points collected for each wire.

Another data set was collected from one horizontal wire on an adaptation of the prototype with one wire frame and two biasing plates. This data set characterized the change in the detector signal as the beam's RF power was attenuated. For this data set, the beam was also imaged using the DRZ film at some of the attenuation settings.

ISBN: 978-3-95450-261-5 ISSN: 2673-7000 doi: 10.18429/JACoW-NAPAC2025-MOP086

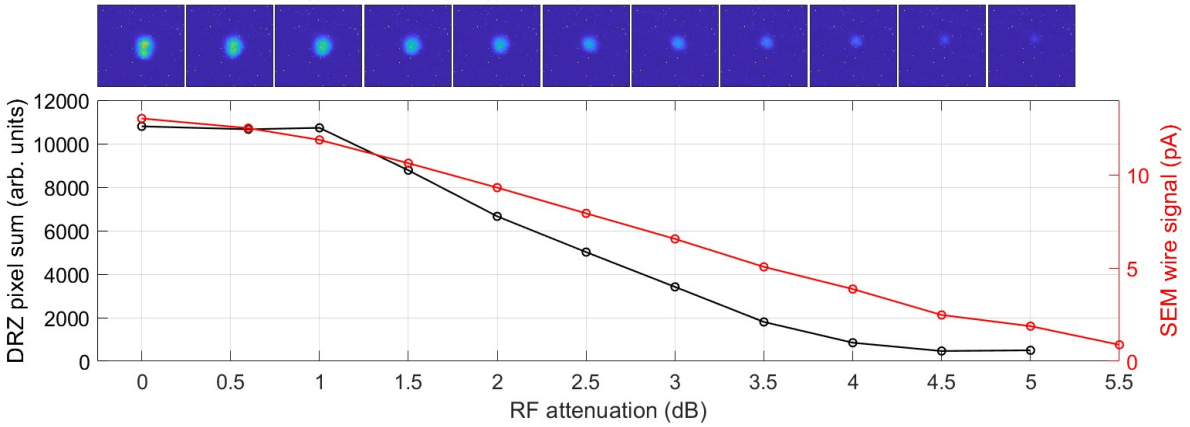

Figure 4: Measurements taken with the DRZ film and one horizontal wire on the SEM grid for different RF power attenuation settings. The axis on the left shows the pixel sum from the DRZ images (at top) corresponding to the region intercepted by the horizontal wire. The axis on the right shows the current signal from the wire in this measurement configuration. Attenuation of the RF power reduces beam charge and energy.

This data set demonstrated the responsiveness of the wire grid to changes in the incoming beam. As the incoming beam's RF power was attenuated, the signal from the measured wire decreased accordingly. This behavior is graphed in Fig. 4, where additionally the beam's profile can be seen growing fainter on the DRZ film.

CONCLUSION

The test of this SEM grid in air at NLCTA showed results comparable to established testing methods. While the current data is sparse, it demonstrates detector signal variation with varying beam power, and allows for the production of a 2D profile based on a Gaussian fit on each wire plane. This particular prototype would need further refining before it could be applied at NorthStar Medical Radioisotopes. Our recommendations for future development include testing the system in vacuum, improving the electronic measurement system to better accommodate more wires, and reducing the form factor of the device.

ACKNOWLEDGEMENTS

The Harvey Mudd College team would like to acknowledge the support of many staff members and professors at Harvey Mudd College, as well as our company liaisons at NorthStar Medical Radioisotopes, Dr. Joshua Peterson-Droogh, Dr. Michael Skulski, and Dr. Brandon Jackson. We would also like to acknowledge the work of our fall semester juniors Damilola Dada and Ella Allgor, and our fall semester advisor Professor Ethan Ritz. Additional thanks to the staff at previous testing locations University of Maryland College Park and Electron Beam Engineering - these tests provided invaluable insights as the design was iterated on throughout the capstone project. Finally, we would like to thank experts on beam diagnostics and physics who graciously took the time to give us advice: Dr. Alexander Saad, Dr. Araceli Navarro Fernandez, Dr. Cameron Duncan, Eric Letcher, Dr. Mariusz Sapinski, Dr. Randy Thurman-Keup, Richard Prokop, and Dr. Victor Scarpine.

REFERENCES

[1] R. M. Prokop, "Target multiwire for the Fermilab Booster Neutrino Beamline", in *Proc. IBIC'23*, Saskatoon, Canada. Sep. 2023, pp. 392-394. doi:10.18429/JACoW-IBIC2023-WEP022

[2] M. Bernard *et al.*, "Secondary Emission Grids for Low and High Energy Electron Beams", in *Proc. EPAC'96*, Sitges, Spain, Jun. 1996, paper TUP058L, pp. 1680-1682.

[3] Radiopharmaceutical Therapy: The Science, https://www.northstarnm.com/radiopharmaceutical-therapy/the-science

[4] Radiopharmaceutical Therapy: Actinium-225, https://www.northstarnm.com/radiopharmaceutical-therapy/actinium-225

[5] Radiopharmaceutical Therapy: Copper-67, https://www.northstarnm.com/radiopharmaceutical-therapy/copper-67

[6] A. N. Fernandez, "Characterization and optimization of CERN Secondary Emission Monitors (SEM) used for beam diagnostics," Bachelor's degree final project, Universitat Politécnica de Catalunya, Barcelona, Spain, 2017, https://hdl.handle.net/2117/105996

[7] J. Yater, "Secondary electron emission and vacuum electronics," *J. Appl. Phys.*, vol. 133, no. 5, p. 050901, 2023. doi:10.1063/5.0130972

[8] A. Shih, J. Yater, C. Hor, and R. Abrams, "Secondary electron emission studies," *Appl. Surf. Sci.*, vol. 111, pp. 251-258, 1997. doi:10.1016/S0169-4332(96)00729-5

[9] L. Conradie, "Beam diagnostics," presented at the Joint ICTP-IAEA Workshop on Electrostatic Accelerator Technologies, Basic Instruments and Analytical Techniques, Trieste, Italy, Oct. 2019, unpublished. https://indico.ictp.it/event/8728/session/8/contribution/32/material/slides/0.pdf

ISBN: 978-3-95450-261-5 ISSN: 2673-7000 doi: 10.18429/JACoW-NAPAC2025-MOP086

[10] X-ray Scintillator Screen 'DRZ', https://www.m-chemical.co.jp/en/products/departments/mcc/ledmat/product/1201037_7550.html